

# Magnetic field strength influence on the reactive magnetron sputter deposition of Ta<sub>2</sub>O<sub>5</sub>

R Hollerweger<sup>1,3</sup>, D Holec<sup>2</sup>, J Paulitsch<sup>1,3</sup>, R Rachbauer<sup>4</sup>, P Polcik<sup>5</sup> and P H Mayrhofer<sup>1,3</sup>

<sup>1</sup> Christian Doppler Laboratory for Application Oriented Coating Development at the Department of Physical Metallurgy and Materials Testing, Montanuniversität Leoben, Franz-Josef-Str. 18, A-8700 Leoben, Austria

<sup>2</sup> Department of Physical Metallurgy and Materials Testing, Montanuniversität Leoben, Franz-Josef-Str. 18, A-8700 Leoben, Austria

<sup>3</sup> Institute of Materials Science and Technology, Vienna University of Technology, A-1040 Vienna, Austria

<sup>4</sup> OC Oerlikon Balzers AG, Iramali 18, LI-9469 Balzers, Principality of Liechtenstein

<sup>5</sup> Plansee Composite Materials GmbH, Siebenbürgerstr. 23, D-86983 Lechbruck am See, Germany

[robert.hollerweger@tuwien.ac.at](mailto:robert.hollerweger@tuwien.ac.at)

**Abstract.** Reactive magnetron sputtering enables the deposition of various thin films to be used for protective as well as optical and electronic applications. However, progressing target erosion during sputtering results in increased magnetic field strengths at the target surface. Consequently, the glow discharge, the target poisoning, and hence the morphology, crystal structure and stoichiometry of the prepared thin films are influenced. Therefore, these effects were investigated by varying the cathode current  $I_m$  between 0.50 and 1.00 A, the magnetic field strength  $B$  between 45 and 90 mT, and the  $O_2/(Ar+O_2)$  flow rate ratio  $\Gamma$  between 0 and 100%. With increasing oxygen flow ratio a sub-stoichiometric TaO<sub>x</sub> oxide forms at the metallic Ta target surface which further transfers to a non-conductive tantalum pentoxide Ta<sub>2</sub>O<sub>5</sub>, impeding a stable DC glow discharge. These two transition zones (from Ta to TaO<sub>x</sub> and from TaO<sub>x</sub> to Ta<sub>2</sub>O<sub>5</sub>) shift to higher oxygen flow rates for increasing target currents. Contrary, increasing the magnetic field strength (e.g., due to sputter erosion) mainly shifts the TaO<sub>x</sub> to Ta<sub>2</sub>O<sub>5</sub> transition to lower oxygen flow rates while marginally influencing the Ta to TaO<sub>x</sub> transition. To allow for a stable DC glow discharge (and to suppress the formation of non-conductive Ta<sub>2</sub>O<sub>5</sub> at the target) even at  $\Gamma = 100\%$  either a high target current ( $I_m \geq 1$  A) or a low magnetic field strength ( $B \leq 60$  mT) is necessary. These conditions are required to prepare stoichiometric and fully crystalline Ta<sub>2</sub>O<sub>5</sub> films.

PACS classification number: 81.15.Cd

Submitted to: Journal of Physics D: Applied Physics

## 1. Introduction

Reactive magnetron sputtering is a widely spread technique to deposit thin compound films on a huge variety of substrate materials. However, to reproducibly deposit high quality coatings a consolidated knowledge on process influencing effects like the target poisoning behaviour and its impact on the plasma conditions is necessary [1–6]. Therefore, many investigations are focusing on improving process controlling parameters such as power supply, power density, reactive gas flow, total pressure, pumping speed or magnetic field strength [2,7,8].

Determining a cathode-voltage-hysteresis as a function of the reactive gas flow gives an easy access to investigate the poisoning behaviour of the cathode material. In general two operating modes can be distinguished: The metallic sputtering mode, established at low reactive gas contents, in which the target surface still indicates the metallic phase, and the poisoned sputtering mode at higher reactive gas contents, in which a compound layer is formed at the target surface [9,10]. Such compounds can negatively affect the discharge properties due to changes in sputter yields, secondary electron emission or conductivity [11,12].

Magnetron sputtering was introduced in the 70ies as it enables a stable glow-discharge at lower chamber pressures than known for diode-sputtering [13]. The magnetic field of the magnetron is responsible for trapping secondary electrons, which are essential for ionizing the gaseous species and consequently for the plasma density. Nevertheless, progressing sputter erosion of the target material results in an increase of the magnetic field strength and hence to a changed discharge behaviour of the target material [14,15].

Tantalum pentoxide,  $\text{Ta}_2\text{O}_5$ , is a promising candidate for optical, electronic, corrosion-protective and biocompatible applications [16–18]. However, the reactive sputtering process is very sensitive to the reactive gas partial pressure used. Therefore Schiller et al. have studied the influence of the sputtering power, total pressure as well as partial pressure on the sputter rate of Ta and Ti in an Ar/ $\text{O}_2$  glow discharge. Based on their results, they have derived a model for the formation of a microscopic (conductive) or macroscopic (insulating) oxide-compound layer on the target surface to describe the radial oxide coverage and the discharge area [19,20].

Within this study, we investigate the influence of the magnetic field strength, the sputtering current and the oxygen gas flow on the poisoning behaviour of a tantalum target. Our results emphasize the need of a well-balanced process especially when considering the change in magnetic field strength due to continuous sputter erosion of the target surface and high oxygen flow rates which are necessary to obtain crystalline and stoichiometric Ta<sub>2</sub>O<sub>5</sub> films even at substrate temperatures of 500°C.

## 2. Experimental:

All depositions and cathode-voltage-hysteresis experiments were performed in a Leybold Heraeus A400-VL laboratory magnetron sputtering device equipped with a 70 dm<sup>3</sup> chamber and a Leybold Turbovac 361 turbo pump (nominal pumping speed of 345 l/sec (nitrogen)). A tantalum target with a diameter of 75 mm (thickness 6mm) and a purity of 99.9% was used and powered by a Leybold/ELAN SSV1.8kW/2-27 DC generator in constant current mode at I<sub>m</sub> = 0.50, 0.75 and 1.00 A.

In order to decrease the radial magnetic field strength B at the target surface from 90 to 60 and 45 mT, austenitic steel plates were used as spacers between the cathode and the permanent magnets, see figure 1. The magnetic field strength was measured using a portable LakeShore 410 Gauss-meter.

Prior to the hysteresis experiments and without ignited plasma, we have calibrated the flows of Ar ( $f_{Ar}$ ) and O<sub>2</sub> ( $f_{O_2}$ ) to reach a constant total pressure of 0.4 Pa. Therefore,  $f_{O_2}$  was stepwise increased from 0 to 23.7 sccm to linearly increase the O<sub>2</sub> partial pressure while simultaneously  $f_{Ar}$  was decreased from 17 to 0 sccm. 30 separate data points were recorded per voltage hysteresis for increasing and subsequently decreasing flow rate  $\Gamma$ , with

$$\Gamma = \frac{f_{O_2}}{f_{Ar} + f_{O_2}} \times 100 .$$

The holding time for every single point was 5 minutes to approach equilibrium discharge conditions.

Tantalum oxide films were deposited on Si stripes ((100) orientation, 20x7x0.38 mm<sup>3</sup>) using a target current of 0.75 A, a radial magnetic field strength of 60 mT, and flow rates of  $\Gamma$  = 50, 77 and 100%.

The substrate temperature was set to 500 °C and the distance to the target surface was 4.5 cm.

Structural investigations were conducted by X-ray diffraction (XRD) analysis in Bragg Brentano geometry using a Bruker D8 diffractometer equipped with a CuK $\alpha$  radiation source. The chemical composition was determined by elastic recoil detection analysis (ERDA) using Cl<sup>7+</sup> ions with an acceleration voltage of 35 MeV by evaluating the resulting spectrum according to Barrada et al. [21]. Fracture cross-sectional scanning electron microscopy (SEM) investigations with an acceleration voltage of 15 kV were conducted with a Zeiss EVO50 for coating morphology studies and thickness evaluations. Prior to these SEM investigations, a thin Au-layer was deposited to increase the conductivity of our samples.

Energies of formation and density of states (DOS) of TaO (NaCl, Fm-3m (225), [22]), TaO<sub>2</sub> (rutile, P42/mnm (136), [23]) and Ta<sub>2</sub>O<sub>5</sub> (orthorhombic structure proposed by Lehovc [24]) were calculated using the Vienna ab initio software package (VASP) [25,26] employing projector augmented wave pseudopotentials [27] and the generalized gradient approximation [28]. The unit cells of TaO, TaO<sub>2</sub> and Ta<sub>2</sub>O<sub>5</sub> contained 8, 6, and 14 atoms, respectively and the used cut-off energy of 800 eV and more than 2000 k-points/atom ensure a minimum accuracy of 1 meV/atom. The energies of formation were calculated as,

$$E_f = E_{TaO_x} - \frac{E_{Ta} + \frac{x}{2} \times E_{O_2}}{1+x}$$

where  $E_{TaO_x}$ ,  $E_{Ta}$  and  $E_{O_2}$  are the total energies of the crystalline TaO<sub>x</sub>, bcc Ta and molecular O<sub>2</sub>, respectively.

### 3. Results and Discussion:

#### 3.1. Voltage hysteresis

Figure 2 shows a voltage hysteresis, at a target current of  $I_m = 0.75$  A and a magnetic field strength of  $B = 90$  mT as a function of the oxygen gas flow  $\Gamma$ . Between  $\Gamma = 0$  and ~65% (first regime, (a)) a voltage peak of ~475 V can be observed at about  $\Gamma = 50\%$ . The increase to this peak value can be attributed to the linear reduction of the Ar flow, oxygen gettering by evaporated metal atoms [29],

chemisorption and implantation of oxygen atoms at the target [29,30], and also to the constriction of the discharge region due to partial poisoning [19]. At the peak, the discharge voltage and the ion density have reached the optimum conditions for restricting further oxidation of the target surface and the constriction of the discharge area has reached its maximum. If even more oxygen is introduced to the chamber, the target coverage increases, the discharge area broadens again and the voltage decreases until the poisoning processes are completed for the whole target surface. Subsequently stable discharge conditions, characterized by an almost constant voltage regime (b), can be observed up to  $\Gamma = 90\%$ , figure 2, and indicate that the formed compound is stable. For higher flow rates, between  $\Gamma = 90$  and  $100\%$  (c), the third regime is characterized again by an increase of the discharge voltage, due to the formation of a different compound layer at the target surface further influencing the target resistance. Upon decreasing the  $O_2$  flow rate the hysteresis can be clearly identified for regime (a) and (c) in figure 2. Moreover, a non-stable DC glow discharge at  $\Gamma = 100\%$  suggests a close to stoichiometric  $Ta_2O_5$  compound formed on the target surface with a low conductivity, whereas the stable conditions within regime (b) suggest that the target surface is fully covered by a conductive substoichiometric  $TaO_x$  phase.

Possible candidates for substoichiometric  $TaO_x$  phases are metastable  $TaO$  and  $TaO_2$  [31]. Therefore, ab initio calculations were performed to obtain information on the conductivity, stability and affinity to oxygen. These calculations yield energies of formation of  $-1.192$  eV/atom ( $-230$  kJ/mol) for  $TaO$ ,  $-2.990$  eV/atom ( $-865$  kJ/mol) for  $TaO_2$  and  $-3.158$  eV/atom ( $-1079$  kJ/mol) for  $TaO_{2.5}$  (for comparison with the other phases we have normalized  $Ta_2O_5$  to  $TaO_{2.5}$ ). These results are in excellent agreement with experimentally obtained values of  $-1023$  kJ/mol [32] and  $-1017$  kJ/mol [33] for  $TaO_{2.5}$ . According to our calculations, the energy gain from  $TaO$  and  $TaO_2$  towards the stable  $TaO_{2.5}$  is  $849$  kJ/mol and  $214$  kJ/mol for  $TaO$  and  $TaO_2$ , respectively. The DOS for these three phases, figures. 3a, b, and c, indicate a shift in the (pseudo) bandgap (marked by the black arrow) towards the Fermi level with increasing oxidation state of Ta from  $TaO$  to  $TaO_2$  to  $Ta_2O_5$ , respectively. For  $TaO$  and  $TaO_2$  there are occupied states at the Fermi level suggesting conductivity. On the other hand,  $Ta_2O_5$

exhibits a bandgap ( $\sim 2.5$  eV) at the Fermi-level, characteristic for an insulating material (please note that density functional theory (DFT) calculations tend to underestimate the bandgap width).

Due to these calculations and the much higher energy of formation for  $\text{TaO}_2$  as compared with  $\text{TaO}$ , combined with the result that regime (b) of figure 2 is characterized by a stable discharge over a wide range of oxygen flow rate, we propose that the properties of the tantalum oxide layer responsible for this regime are comparable to metastable  $\text{TaO}_2$ .

Moreover, the voltage increase (figure 2) from  $\sim 310\text{V}$  at  $\Gamma = 0\%$  to  $\sim 410\text{V}$  at  $\Gamma = 75\%$  to  $\sim 475\text{V}$  at  $\Gamma = 100\%$ , indicates decreasing secondary electron emission (SEE) yields for Ta,  $\text{TaO}_x$  and  $\text{Ta}_2\text{O}_5$  covered target surfaces, respectively, which is known for the Ta –  $\text{Ta}_2\text{O}_5$  system [34].

*3.1.1. Current variation.* With increasing sputtering current  $I_m$  from 0.50 to 0.75 to 1.00 A the three discharge regimes are clearly shifted to higher oxygen flow rates, figure 4. Furthermore, the regime with a stable discharge voltage (between the first and the second hysteresis) covers a broader oxygen flow rate with increasing sputtering current. For  $I_m = 1$  A, the second hysteresis effect due to the formation of an insulating  $\text{Ta}_2\text{O}_5$  cannot be observed allowing for stable discharge conditions even for 100% of oxygen flow rate. Additionally, the second hysteresis, due to the formation of  $\text{Ta}_2\text{O}_5$ , clearly widens with decreasing target currents. This can be explained by the reduced particle bombardment (density) and energy caused by decreasing target current and voltage, and hence  $\text{Ta}_2\text{O}_5$  stabilizes earlier during increasing flow rates, and (when formed) is stable to lower  $\Gamma$  values during decreasing flow rates. The shift of the first hysteresis (formation of  $\text{TaO}_x$ ) to lower oxygen flow rates with decreasing sputtering current is also based on the decreasing particle bombardment and consequently decreasing sputtering rate.

*3.1.2. Magnetic field strength variation.* The effect of progressing target erosion is investigated by modifying the magnetic field strength  $B$  at the surface (see experimental). Figures 5a and b show the discharge voltage behaviour for radial magnetic field strengths  $B$  of 45, 60, and 90 mT at a constant target current  $I_m$  of 0.50 and 0.75 A, respectively. Increasing magnetic field strengths at constant target currents shifts the target voltage characteristics to lower values as more electrons are captured and more particles are ionized. Whereas the magnetic field strength variation (within the investigated

ranges) has no significant influence on the position of the first hysteresis voltage peak, the second hysteresis is strongly influenced in shape and position. For both target current conditions of  $I_m = 0.50$  and  $0.75$  A no second hysteresis can be observed for the lower magnetic field strengths  $B$  of  $45$  and  $60$  mT, see figures 5a and b. This indicates that under these conditions no  $Ta_2O_5$  compound layer is formed at the target surface. In this case we assume the cohesive energy of the present phase on the target surface, which is in general much lower for a metal than for the particular oxide, to play a major role. Consequently, mainly the density of the impinging ions is influencing the flow rate position of the Ta to  $TaO_x$  hysteresis. Furthermore, the data also suggests that the second transition zone from  $TaO_x$  to  $Ta_2O_5$  is additionally to the density also influenced by the energy of the target impinging particles.

In agreement to the voltage dependence of the  $TaO_x$  formation, which suggests decreasing SEE yields from Ta to  $TaO_x$  to  $Ta_2O_5$  (last paragraph in section 3.1) the above discussed magnetic field strength variation suggests decreasing secondary electron energies from Ta to  $TaO_x$ . Thus, the dependence of the discharge voltage on the magnetic field strength is more pronounced for the metallic Ta target surface at  $\Gamma = 0\%$  as compared with the oxidized state.

These investigations clearly demonstrate that the discharge and consequently the poisoning behaviour of the target are substantially influenced by the target erosion induced increase of the magnetic field strength, especially when operating at higher oxygen flow rates and lower sputtering currents.

### 3.2. Film deposition

Based on the previous studies we have chosen the settings of  $I_m = 0.75$  A and  $B = 60$  mT for the preparation of tantalum oxide films using oxygen flow rates of  $50$ ,  $77$  and  $100\%$ , as these allow for a stable deposition process even at higher oxygen flow rates. The comparison of the cathode voltage and deposition rate as a function of the oxygen flow rate, figure 6, clearly exhibits a maximum deposition rate of  $110$  nm/min, when using the oxygen flow rate slightly above the peak voltage. Increasing the oxygen flow rate  $\Gamma$  to  $77$  and  $100\%$  causes the deposition rate to decrease to  $15$  and  $10$  nm/min,

194 respectively. The decrease from 110 to 15 nm/min can mainly be related to the different target surface  
195 condition, which is still metal dominated at the voltage peak for  $\Gamma = 50\%$ , but completely covered by a  
196  $\text{TaO}_x$  compound layer for  $\Gamma = 77\%$ . Further decreased deposition rates of 10 nm/min when using  $\Gamma =$   
197 100% are probably caused by different sputtering yields of Ar and  $\text{O}_2$ , as proposed by Yamamura et.  
198 al. [35], as well as due to changes in crystallinity and stoichiometry of the coatings, see next  
199 paragraph.

200 The coating prepared at  $\Gamma = 50\%$  exhibits a dense columnar crystalline structure for the  $\sim 10\ \mu\text{m}$  thick  
201 top region, preceded by a featureless, amorphous-like morphology up to a layer thickness of the first  
202  $\sim 5\ \mu\text{m}$ , figure 7a. This was confirmed when decreasing the deposition time from 120 to 5 min, as  
203 thereby the  $\sim 1\ \mu\text{m}$  thin film exhibits only a featureless morphology, figure 7b. This featureless near-  
204 substrate region of the coating decreases with increasing oxygen flow rate and decreasing deposition  
205 rate, and is  $\sim 0.5\ \mu\text{m}$  for  $\Gamma = 77\%$  and essentially zero for  $\Gamma = 100\%$ , see figures. 8a and b. XRD  
206 investigations, figure 9, confirm the crystalline nature of a highly texturized (110)/(200) orthorhombic  
207  $\text{Ta}_2\text{O}_5$  structure, in the outer most part of the coatings prepared at  $\Gamma = 50\%$ , pattern (a). When  
208 decreasing the layer thickness to  $\sim 1\ \mu\text{m}$ , only an X-ray amorphous response is obtained, pattern (b), in  
209 agreement to the SEM fracture cross section, figure 7b. The coatings prepared at higher oxygen flow  
210 rates,  $\Gamma = 77$  and 100%, exhibit an orthorhombic  $\text{Ta}_2\text{O}_5$  structure as well. However, with increasing  
211 oxygen flow rate the preferred orientation changes towards (001), see figure 9 pattern (c) and (d). The  
212 chemical compositions of our coatings, table 1, suggest that only for  $\Gamma = 100\%$  a stoichiometric  $\text{Ta}_2\text{O}_5$   
213 with  $\text{O}/\text{Ta} = 2.5$ , is obtained, indicating that high oxygen partial pressures are needed to form  
214 crystalline stoichiometric  $\text{Ta}_2\text{O}_5$  as proposed by Ritter [36]. The coatings synthesized at  $\Gamma = 50$  and  
215 77% are slightly substoichiometric, with an O/Ta ratio of 2.33 and 2.35, respectively.



#### 4. Summary and conclusions

Voltage hysteresis of a Ta target in an Ar/O<sub>2</sub> atmosphere at three different sputtering currents and magnetic field strengths were investigated with respect to its target poisoning behaviour as well as resulting film structure and morphology. We indicated three main sputtering regions which are dominated by the target surface transition from Ta to TaO<sub>x</sub>, a stable conductive TaO<sub>x</sub> region and finally the transition of TaO<sub>x</sub> to insulating Ta<sub>2</sub>O<sub>5</sub>. All three regions are strongly influenced by the cathode current used. Variations of the magnetic field strength mainly affect the second and third regime, whereas the first one does not change significantly. This can be related to the difference in cohesive energies of metallic Ta and Ta-oxide. XRD investigations of deposited Ta-oxides at 50, 77, and 100% oxygen flow rate exhibit a pentoxide structure. However, stoichiometric films could only be obtained at  $\Gamma = 100\%$ , whereas the O-to-Ta rate of the coatings prepared with  $\Gamma = 50$  and 77% is slightly sub-stoichiometric with 2.33 and 2.35 respectively. These coatings also exhibit an amorphous phase content next to the substrate interface.

Our investigations demonstrate the pronounced influence of the magnetic field strength, which may change due to e.g. target erosion, on the target poisoning and discharge behaviour, especially at high reactive gas flow ratios, which are necessary to obtain stoichiometric crystalline Ta<sub>2</sub>O<sub>5</sub> coatings.

#### 5. Acknowledgement

This work has been supported by the European Community as an Integrating Activity 'Support of Public and Industrial Research Using Ion Beam Technology (SPIRIT)' under EC contract no. 227012 as well as by the Start Program (Y 371) of the Austrian Science Fund (FWF) and the "Christian Doppler" research association.

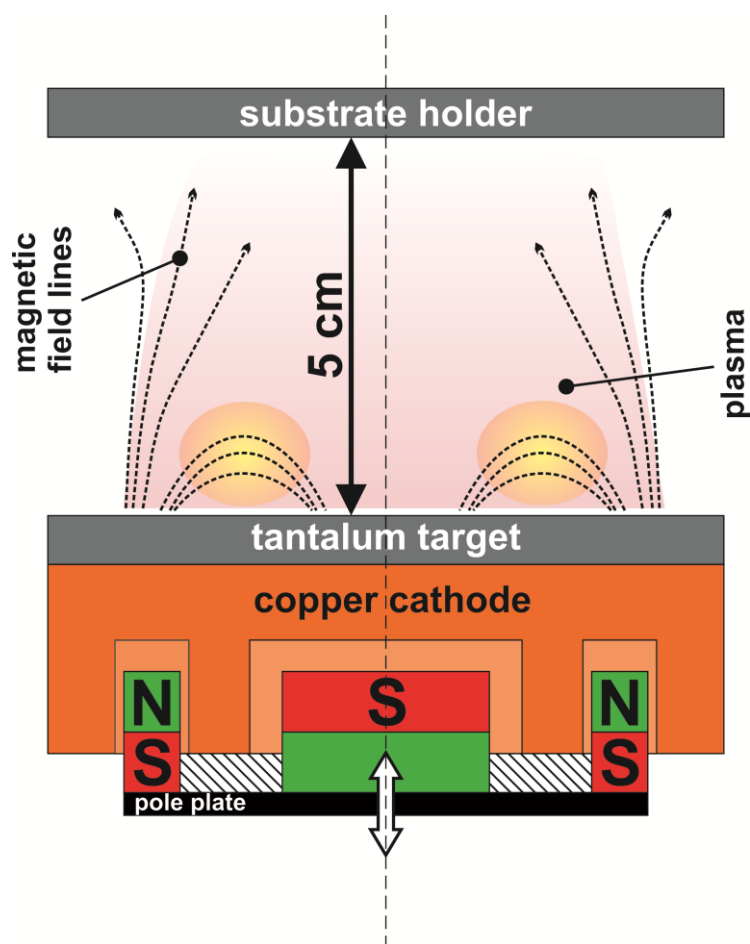
239 **References:**

- 240 [1] Güttler D, Grötzschel R and Möller W 2007 Lateral variation of target poisoning during  
241 reactive magnetron sputtering *Appl. Phys. Lett.* **90** 263502
- 242 [2] Schiller S, Beister G and Sieber W 1984 Reactive high rate D.C. sputtering: Deposition rate,  
243 stoichiometry and features of TiO<sub>x</sub> and TiN<sub>x</sub> films with respect to the target mode *Thin Solid*  
244 *Films* **111** 259–68
- 245 [3] Mohamed S 2003 Correlation between structure, stress and optical properties in direct current  
246 sputtered molybdenum oxide films *Thin Solid Films* **429** 135–43
- 247 [4] Westwood W D 1974 Effect of pressure on the properties of reactively sputtered Ta[sub  
248 2]O[sub 5] *J. Vac. Sci. Technol.* **11** 381
- 249 [5] Kadlec S 1987 Influence of the pumping speed on the hysteresis effect in the reactive  
250 sputtering of thin films *Vacuum* **37** 729–38
- 251 [6] Kusano E 1991 An investigation of hysteresis effects as a function of pumping speed,  
252 sputtering current, and O<sub>2</sub>/Ar ratio, in Ti-O<sub>2</sub> reactive sputtering processes *J. Appl. Phys.* **70**  
253 7089
- 254 [7] Baroch P, Musil J, Vlcek J, Nam K H and Han J G 2005 Reactive magnetron sputtering of  
255 TiO<sub>x</sub> films *Surf. Coat. Technol.* **193** 107–11
- 256 [8] Münz W, Heimbach J and Reineck S 1981 Reactive high rate sputtering of oxides *Thin Solid*  
257 *Films* **86** 175–82
- 258 [9] Sproul W D, Christie D J and Carter D C 2005 Control of reactive sputtering processes *Thin*  
259 *Solid Films* **491** 1–17
- 260 [10] Safi I 2000 Recent aspects concerning DC reactive magnetron sputtering of thin films: a review  
261 *Surf. Coat. Technol.* **127** 203–18
- 262 [11] Depla D, Mahieu S and Gryse R De 2009 Magnetron sputter deposition: Linking discharge  
263 voltage with target properties *Thin Solid Films* **517** 2825–39
- 264 [12] Berg S and Nyberg T 2005 Fundamental understanding and modeling of reactive sputtering  
265 processes *Thin Solid Films* **476** 215–30
- 266 [13] Westwood W 2003 *Sputter deposition* (New York: AVS)
- 267 [14] Furuya A and Hirono S 2000 Suppression of deposition rate variations and of structural  
268 changes in the characteristics of magnetic films deposited by magnetically controlled  
269 magnetron sputtering *J. Appl. Phys.* **87** 939–44
- 270 [15] Furuya A and Hirono S 1990 Target magnetic-field effects on deposition rate in rf magnetron  
271 sputtering *J. Appl. Phys.* **68** 304–10
- 272 [16] Ritz A 2003 TaTiO<sub>x</sub> layers prepared by magnetron sputtering from separate metal targets *Surf.*  
273 *Coat. Technol.* **174-175** 651–4

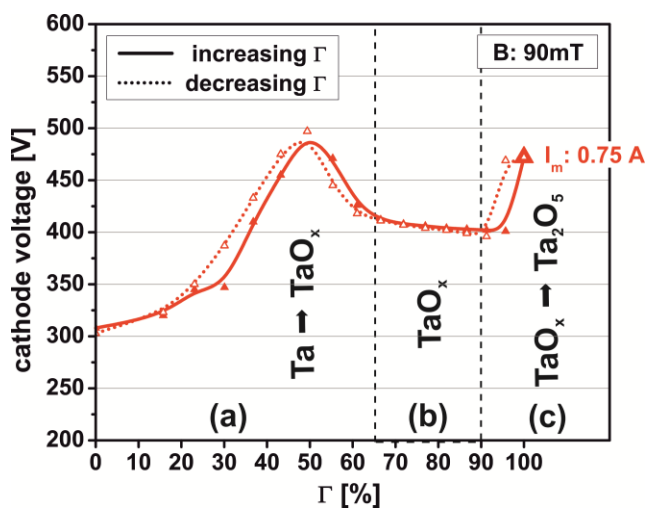
- 274 [17] Chaneliere C, Autran J L, Devine R A B and Balland B 1998 Tantalum pentoxide (Ta<sub>2</sub>O<sub>5</sub>) thin  
275 films for advanced dielectric applications *Mater. Sci. Eng. R*: **22** 269–322
- 276 [18] Donkov N, Zykova A, Safonov V, Rogowska R and Smolik J 2011 TANTALUM  
277 PENTOXIDE CERAMIC COATINGS DEPOSITION ON Ti<sub>4</sub>Al<sub>6</sub>V SUBSTRATES FOR  
278 BIOMEDICAL APPLICATIONS *Probl. At. Sci. Technol.* 131
- 279 [19] Schiller S, Heisig U, Steinfeld K and Strümpfel J 1979 Reactive D.C. sputtering with the  
280 magnetron-plasmatron for tantalum pentoxide and titanium dioxide films *Thin Solid Films* **63**  
281 369–75
- 282 [20] Schiller S, Heisig U, Steinfeld K, Strümpfel J and Sieber W 1981 Reactive D.C. High-rate  
283 Sputtering with the Magnetron/Palsmatron for Industrial Applications *Vak. Tech.* **30** 3–14
- 284 [21] Barradas N P, Jeynes C and Webb R P 1997 Simulated annealing analysis of Rutherford  
285 backscattering data *App. Phys. Lett.* **71** 291
- 286 [22] Schönberg N, Overend W G, Munthe-Kaas A and Sörensen N A 1954 An X-Ray Investigation  
287 of the Tantalum-Oxygen System. *Acta Chem. Scand.* **8** 240–5
- 288 [23] Terao N 1967 Structure des Oxides de Tantale *Jpn. J. Appl. Phys.* **6** 21–34
- 289 [24] Lehovc K 1964 Lattice structure of  $\beta$ -Ta<sub>2</sub>O<sub>5</sub> *J. Less Common Met.* **7** 397–410
- 290 [25] Kresse G and Hafner J 1993 Ab initio molecular dynamics for liquid metals *Phys. Rev. B* **47**  
291 558–61
- 292 [26] Kresse G and Furthmüller J 1996 Efficient iterative schemes for ab initio total-energy  
293 calculations using a plane-wave basis set *Phys. Rev. B* **54** 11169–86
- 294 [27] Kresse G and Joubert D 1999 From ultrasoft pseudopotentials to the projector augmented-wave  
295 method *Phys. Rev. B* **59** 1758–75
- 296 [28] Wang Y and Perdew J 1991 Correlation hole of the spin-polarized electron gas, with exact  
297 small-wave-vector and high-density scaling *Phys. Rev. B* **44** 13298–307
- 298 [29] Depla D and Gryse R De 2004 Target poisoning during reactive magnetron sputtering: Part II:  
299 the influence of chemisorption and gettering *Surf. Coat. Technol.* **183** 190–5
- 300 [30] Depla D and Gryse R De 2004 Target poisoning during reactive magnetron sputtering: Part I:  
301 the influence of ion implantation *Surf. Coat. Technol.* **183** 184–9
- 302 [31] Pies W and Weiss A 1975 The Landolt-Börnstein Database, Key Element: O. Part 1 *Landolt-  
303 Börnstein - Group III Condensed Matter Numerical Data and Functional Relationships in  
304 Science and Technology* vol 7b1, ed K-H Hellwege and A M Hellwege (Berlin/Heidelberg:  
305 Springer-Verlag) pp 451 – 461
- 306 [32] Blachnik R 1998 *Taschenbuch für Chemiker und Physiker* (Berlin: Springer)
- 307 [33] Perry R and Green D 1997 *Perry's chemical engineers' handbook* (New York: McGraw-Hill)
- 308 [34] Ngaruiya J M, Venkataraj S, Drese R, Kappertz O, Leervad Pedersen T P and Wuttig M 2003  
309 Preparation and characterization of tantalum oxide films produced by reactive DC magnetron  
310 sputtering *physica status solidi (a)* **198** 99–110

- 311 [35] Yamamura Y and Ishida M 2003 Simulation of oxide sputtering and SIMS depth profiling of  
312 delta-doped layer *Appl. Surf. Sci.* **203-204** 62–8
- 313 [36] Ritter E 1966 Deposition of Oxide Films by Reactive Evaporation *J. Vac. Sci. Technol.* **3** 225
- 314 [37] *Powder Diffraction File 01-089-2843* PDF-2/Release 2007, International Center for Diffraction  
315 Data
- 316

317 **Figures:**



318  
 319 Figure 1: Sectional schematic of the used unbalanced magnetron system. The cross-striped area  
 320 indicates the austenitic steel spacer sheets.



321  
 322 Figure 2: Cathode voltage hysteresis indicating the three main target poisoning regimes: (a) transition  
 323 from Ta to  $\text{TaO}_x$ , (b) region of stable  $\text{TaO}_x$ , and (c) transition from  $\text{TaO}_x$  to  $\text{Ta}_2\text{O}_5$ .

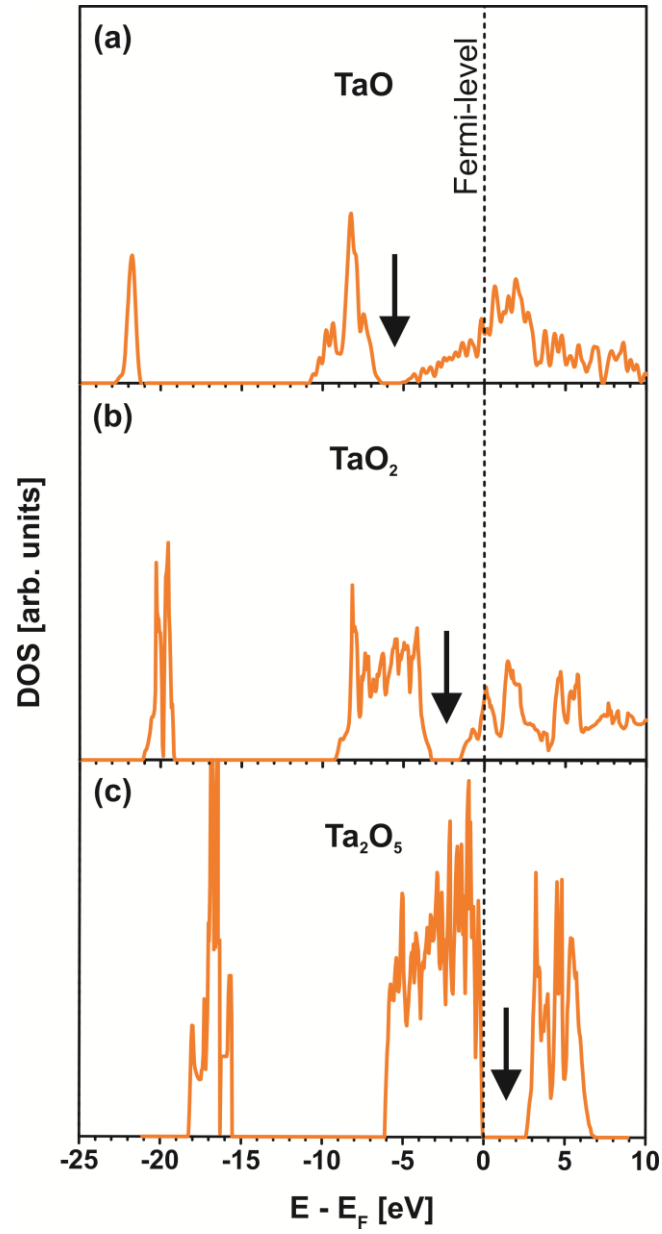


Figure 3: Total density of states (DOS) of (a) TaO, (b) TaO<sub>2</sub>, and (c) Ta<sub>2</sub>O<sub>5</sub>. The vertical arrows indicate the (pseudo-) bandgap.

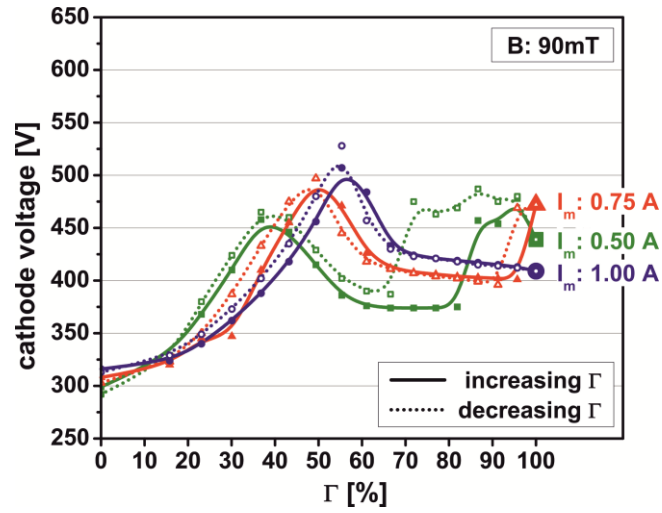


Figure 4: Cathode voltage hysteresis at a constant radial magnetic field strength of 90 mT and target currents of 0.50, 0.75, and 1.00 A.

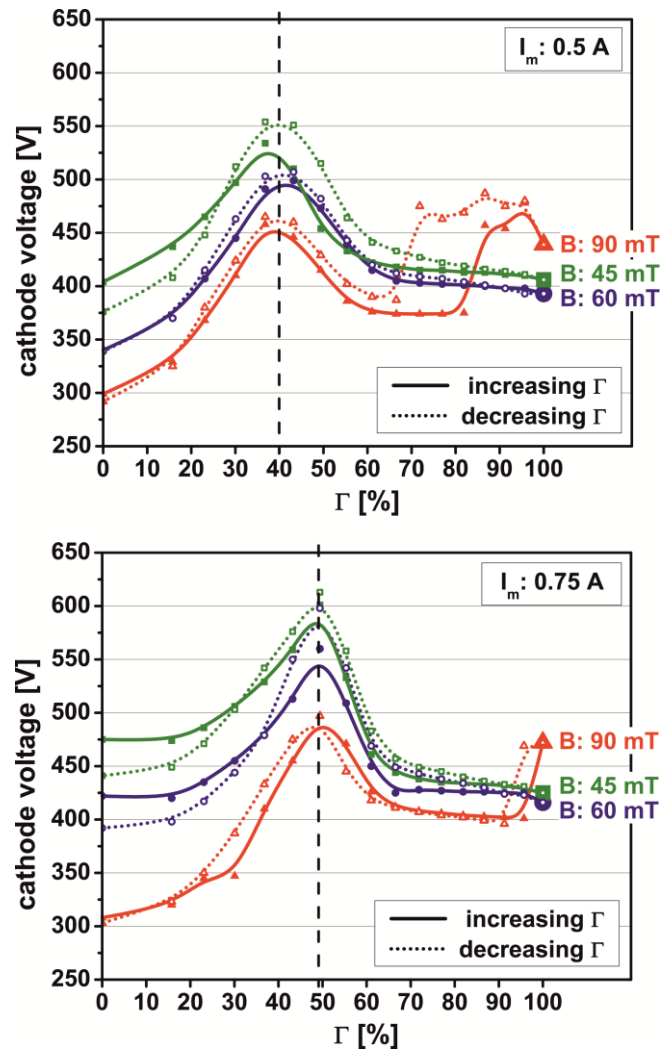


Figure 5: Cathode voltage hysteresis for magnetic field strengths of 45, 60 and 90 mT at target currents  $I_m$  of (a) 0.50 and (b) 0.75 A.

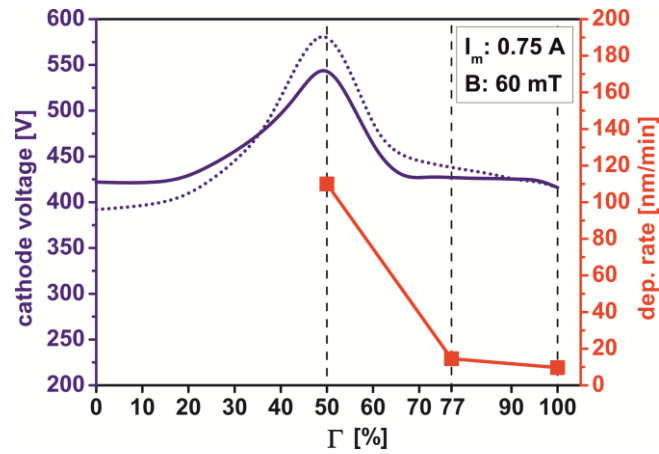


Figure 6: Cathode voltage hysteresis used for film deposition and resulting deposition rates for  $I_m = 0.75$  A and  $B = 60$  mT.

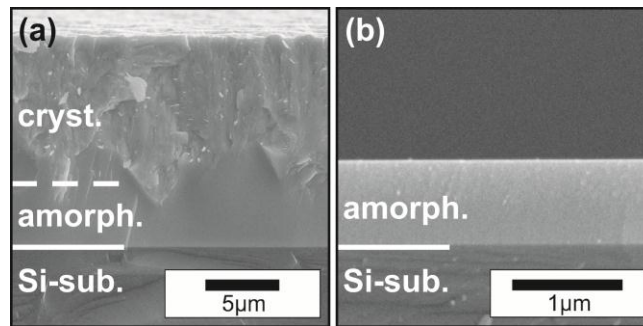


Figure 7: Cross-sectional SEM micrographs of tantalum oxide films deposited at  $\Gamma = 50\%$  for deposition times of (a) 120 min and (b) 5 min.

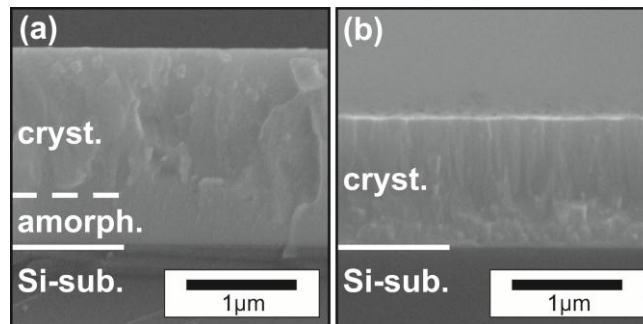
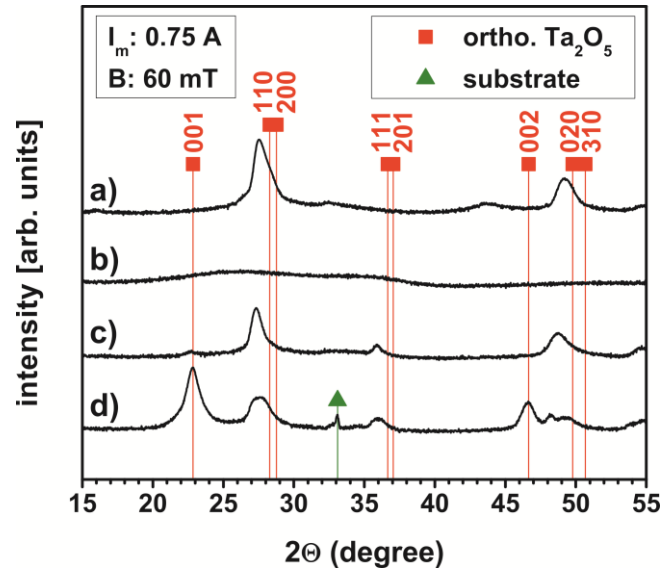


Figure 8: Cross-sectional SEM micrographs of tantalum oxide films deposited at (a)  $\Gamma = 77\%$  and (b)  $100\%$  for a deposition time of 120 min.





342

343

344

345

Figure 9: XRD patterns for tantalum oxide films deposited at (a)  $\Gamma = 50\%$  for 120 min, (b)  $\Gamma = 50\%$  for 5 min, (c)  $\Gamma = 77\%$  for 120 min, and (d)  $\Gamma = 100\%$  for 120 min (indexed after Lehovc et. al. [37]). The corresponding SEM cross-sections are shown in Figures. 7a, b and Figures. 8a, b, respectively.

346 **Tables**

347 **Table 1.** ERDA evaluated chemical composition of Ta<sub>2</sub>O<sub>5</sub> thin films

$\Gamma$ (%)	Ta (at%)	O (at%)	O/Ta (ratio)
50	$30.00 \pm 0.1$	$70.00 \pm 0.7$	$2.33 \pm 0.03$
77	$29.83 \pm 0.1$	$70.17 \pm 0.7$	$2.35 \pm 0.03$
100	$28.30 \pm 0.1$	$71.70 \pm 0.7$	$2.53 \pm 0.03$
stoichiometric	28.57	71.43	2.5

348